Angela Stallone[1], Jacopo Selva[2], Louise Cordrie[1], Licia Faenza[1], Alberto Michelini[3], and Valentino Lauciani[3]

[1]Istituto Nazionale di Geofisica e Vulcanologia INGV, Seismology, Bologna, Italy
[2]University of Naples, Federico II, Dept. of Earth, Environmental, and Resources Sciences, Napoli, Italy
[3]Istituto Nazionale di Geofisica e Vulcanologia INGV, Seismology, Rome, Italy

April 12, 2024

`ProbShakemap` v1.0: a Python toolbox propagating source uncertainty to ground motion prediction for urgent computing applications

Angela Stallone[1], Jacopo Selva[2,1], Louise Cordrie[1], Licia Faenza[1], Alberto Michelini[3], and Valentino Lauciani[3]

[1]Istituto Nazionale di Geofisica e Vulcanologia INGV, Seismology, Bologna, Italy
[2]University of Naples, Federico II, Dept. of Earth, Environmental, and Resources Sciences, Napoli, Italy
[3]Istituto Nazionale di Geofisica e Vulcanologia INGV, Seismology, Rome, Italy

Correspondence: Jacopo Selva (jacopo.selva@unina.it)

Abstract. Seismic urgent computing enables early assessment of an earthquake's impact by delivering rapid simulation-based ground-shaking forecasts. This information can be used by local authorities and disaster risk managers to inform decisions for rescue and mitigation activities in the affected areas. Uncertainty quantification for urgent computing applications stands as one of the most challenging tasks. Present-day practice accounts for the uncertainty stemming from Ground Motion Models (GMMs), but neglects the uncertainty originating from the source model, which, in the first minutes after an earthquake, is only known approximately. In principle, earthquake source uncertainty can be propagated to ground motion predictions with physics-based simulations of an ensemble of earthquake scenarios capturing source variability. However, full ensemble simulation is unfeasible under emergency conditions with strict time constraints. Here we present `ProbShakemap`, a Python toolbox that generates multi-scenario ensembles and delivers ensemble-based forecasts for urgent source uncertainty quantification. The toolbox implements GMMs to efficiently propagate source uncertainty from the ensemble of scenarios to ground motion predictions at a set of Points of Interest (POIs), while also accounting for model uncertainty (by accommodating multiple GMMs, if available) along with their intrinsic uncertainty. `ProbShakemap` incorporates functionalities from two open-source toolboxes routinely implemented in seismic hazard and risk analyses: the USGS `ShakeMap` software and the `OpenQuake-engine`. `ShakeMap` modules are implemented to automatically select the set and weights of GMMs available for the region struck by the earthquake, whereas the `OpenQuake-engine` libraries are used to compute ground shaking over a set of points by randomly sampling the available GMMs. `ProbShakemap` provides the user with a set of tools to explore, at each POI, the predictive distribution of ground-motion values encompassing source uncertainty, model uncertainty and the inherent GMMs variability. Our proposed method is quantitatively tested against the 30 October 2016 Mw 6.5 Norcia, and the 6 February 2023 Mw 7.8 Pazarcik earthquakes. We also illustrate the differences between `ProbShakemap` and `ShakeMap` output.

1 Introduction

Seismic Urgent Computing (UC) (Beckman et al., 2007; Beckman, 2008; Grandinetti, 2008; Leong and Kranzlmüller, 2015) relies on time-critical simulations to estimate the potential hazard of an earthquake shortly after its occurrence (on the order of minutes to hours). This information is of utmost importance for local authorities and disaster risk managers to reduce casualties, manage rescue operations and mitigate financial loss.

Given the inherent uncertainty of forecasting nonlinear processes, ensemble simulations of multiple scenarios are preferred over a purely deterministic approach (Murphy, 1993; Molteni et al., 1996; Sparks, 2003; Gneiting and Raftery, 2005; Selva et al., 2021b; Folch et al., 2023). In the context of seismic UC, the hazard is quantified in terms of ground shaking intensities. In principle, ground shaking can be predicted by 3D modelling of seismic wave propagation for an ensemble of multiple earthquake sources (Ejarque et al., 2022; Folch et al., 2023). However, ensemble-based uncertainty quantification represents a main challenge. While physics-based numerical simulations can provide accurate and physically meaningful ground-shaking scenarios (provided that the source and velocity models are accurate enough), full ensemble simulations are currently unfeasible because of the strict time constraints imposed by UC applications (Selva et al., 2021a; Guérin-Marthe et al., 2021). In this case, to optimize the utilization of the computational resources while still spanning the entire source variability, simulations are run only for a subset of ensemble members, identified with dimensionality reduction techniques (Team, 2010; Feenstra, 1998). Beyond the challenges specific to UC applications, the application of physics-based simulations of ground motions for three-dimensional structures is hampered by their high computational demand at the frequencies of engineering interest and the large uncertainties in the velocity structure, especially at shallow depths (Douglas and Aochi, 2008).

An alternative to numerical simulations of ground motion scenarios lies in the use of Ground Motion Models (GMMs), also known as Ground Motion Prediction Equations (GMPEs). GMMs are empirically-based parametric models that return estimates of the median and variability of expected ground motions at a given site. Over the years, however, the implementation of GMMs for seismic hazard assessment has encountered growing criticism given the significant uncertainties in ground-motion estimates. This owes to the limited data (Douglas, 2003, 2010a, b), the wide variety of empirical relationships for a given area (Gasparini et al., 2007; Douglas, 2020) and the ergodic assumption (Anderson and Brune, 1999). Nevertheless, given the high computational cost of physics-based simulations, GMMs still represent the key ingredient of seismic hazard assessment. For seismic UC, GMMs are routinely implemented in the US Geological Survey's (USGS) `ShakeMap` system (Worden et al., 2020), which is the most widely adopted software for a quick post-earthquake estimation of ground shaking intensities. At its core, `ShakeMap` software is a seismologically-based data interpolator that relies on parametric ground motion data, GMMs and local site amplifications. Maps of `ShakeMap` uncertainties are calculated based on the spatial variability of peak ground motions (which is assumed to be zero at the recording stations and increases with distance) and on the total variability of the implemented GMMs (Worden et al., 2018; Engler et al., 2022). These maps are generated for a single earthquake source, with initial parameter estimates typically available within 30 minutes of the earthquake's origin time. A better constraint of the source parameters is achievable only after several hours, once new data become available, and preliminary finite fault

inversions are performed. This implies that, at the time span of urgent decision-making (minutes to hours), uncertainty about the earthquake source is highest.

Here we present `ProbShakemap`, a Python toolbox that efficiently quantifies and propagates ensemble-based source uncertainty while accounting for inter-model (among different GMMs) and intra-model (within each GMMs) uncertainties. We present two proofs of concept aimed at testing `ProbShakemap` in the context of UC applications: the Mw 6.5, 2016 Norcia and the Mw 7.8, 2023 Pazarcik earthquakes.

`ProbShakemap` exploits both the USGS `ShakeMap` software (Worden et al., 2020) and the `OpenQuake-engine` (the open-source software for seismic hazard and risk analyses of the Global Earthquake Model, GEM; Pagani et al., 2014a). `ProbShakemap` generates an ensemble of scenarios consisting of finite faults with variable geometry and focal mechanism. These source scenarios are compatible with the event under consideration, in that they are based on early estimations of magnitude and hypocentre while also relying on prior information on faults and past seismicity in the region (Selva et al., 2021b). The scenarios, along with the user-provided target points (Points of Interest, POIs), are then converted into a format suitable for the `OpenQuake-engine`. For each earthquake scenario, `ProbShakemap` generates a distribution of ground motion fields at each target point by sampling the GMMs probability distributions proportionally to their weight. In the final stage, the predictions are aggregated into a stacked distribution at each target point. Alike the USGS `ShakeMap` software, `ProbShakemap` samples the GMMs inherent variability. Differently from the USGS `ShakeMap` software, it also accounts for earthquake source uncertainty. `ProbShakemap` does not rely on ground-motion recordings and derived peak ground motion parameters, but only on the ensemble of source scenarios and the GMMs available for the area struck by the earthquake. The output consists of Probability Density Functions (PDFs) forecasting the maximum shaking value (PGA, PGV, SA(0.3), SA(1.0), SA(3.0)) at all target points. These PDFs can be explored with three "prob tools", aiding the user to visualize and summarize the predictive ground-motion distributions at the entire set or a subset of target points.

2 Method

2.1 ProbShakemap: the toolbox

`ProbShakemap` relies on `ShakeMap` and `OpenQuake` Python-based packages. The code can be run locally for a relatively small number of earthquake source scenarios (in the order of a few thousand), but it is recommended to exploit HPC resources and parallelism for large ensembles and/or to enhance code performance. The `ProbShakemap` package includes `SeisEnsMan`, a tool for generating an ensemble of K source scenarios compatible with faults and past seismicity that occurred in the region affected by the event under consideration. The user selects the optimal value for K, and it is recommended to perform trial-and-error tests with progressively larger ensemble sizes. The user needs to provide an estimate of the magnitude and hypocenter of the event. This can be input following two approaches: (1) an automatic search from the "Early-Est" (Bernardi et al., 2015) retrieves the magnitude and hypocenter information with their associated uncertainty matrix; (2) the user can fill in the model provided in input with its own information. Without any additional input information, `SeisEnsMan` generates ensemble scenarios by selecting the source parameters in a hierarchical order: at each level, the parameter space is

defined by a Probability Density Function (PDF) conditioned to the parameters' realisations at the higher levels of the hierarchy. This implies that, at any given level, the realization of a parameter is independent of the parameters at lower levels. Following Selva et al. (2016); Basili et al. (2021); Selva et al. (2021b), four hierarchical levels are defined: (1) Moment magnitude; (2) Hypocentral coordinates (x, y, z); (3) Fault geometry described by strike, dip and average rake; (4) Rupture area and slip derived using scaling laws based on magnitude and rake (Leonard, 2014). The moment magnitude PDF is a normal density function centered on the first magnitude estimate with a standard deviation of 0.3. The hypocenter PDF corresponds to a 3D multivariate Gaussian function centered on the first estimate of the hypocenter with a variance in the 3 directions of 10 km^2. The 3-angle strike-dip-rake PDF corresponds to local probabilistic laws conditioned on the previously picked magnitude and position. It is based on long-term information about local historical seismicity and known faults (see supplementary material in Selva et al., 2016). The choice of the prior model for the 3-angle is automated, with the selection being made between a Mediterranean (Basili et al., 2019, 2021) and a global seismicity model (Taroni and Selva, 2021), based on the earthquake location. Finally, the fault length and the slip are deducted from scaling laws (more details can be found in Selva et al. (2021b)). The following parameterization is used to define each scenario of the ensemble: magnitude, longitude, latitude, hypocenter depth (km), strike, dip, rake, fault area (L*W, km^2), fault length (L, km), slip (m).

`ProbShakemap` reads a file (Table 1) containing the `Shakemap` ID of the event and the input parameters required by the `OpenQuake` modules (for more details, we refer the reader to the `OpenQuake` manual; Pagani et al., 2014b). An example of the input file is provided in the GitHub repository of the `ProbShakemap` toolbox (`INPUT_FILES/input_file.txt`). As a first step, `ProbShakemap` converts each source scenario in the ensemble to an `OpenQuake BaseRupture` object representing a single earthquake rupture.

Subsequently, it proceeds to calculate, for each rupture configuration and for each GMM, the ground-motion mean $\boldsymbol{\mu} = (\mu_1, \mu_2, ..., \mu_S)$ and an array of standard deviations for all POIs $s = (1, 2, ..., S)$, calling the `context_maker.get_mean_stds` method from `OpenQuake`. Each GMM provides indeed a set of equations to compute the mean and standard deviation of the lognormal distribution representing ground motion variability at a specific location, given an earthquake rupture (Atik et al., 2010). The array of standard deviations comprises the total standard deviation σ and its two components, τ (Inter-Event Standard Deviation) and ϕ (Intra-Event Standard Deviation).

The total GMM variability is given by the sum of the $\boldsymbol{\epsilon_\tau}$ and $\boldsymbol{\epsilon_\phi}$, the inter- and intra-event variability, respectively (Atik et al., 2010; Worden et al., 2018). The inter-event variability $\boldsymbol{\epsilon_\tau}$ is constant over the POIs as it only depends on earthquake-to-earthquake variability described by the cross-correlation model defined in input by the user. It is modeled as a random variable that follows a standard univariate (log-)normal distribution (Eq. (1)). On the other hand, the intra-event variability changes across the POIs as it reflects the spatial correlation model (ρ) selected by the user. It is modeled as a two-dimensional random field following a multivariate zero-mean (log-)normal distribution with a covariance matrix Σ describing spatial correlation (Eq. (2)). Σ reduces to a diagonal matrix when no correlation in the intra-event variability is considered.

$$\boldsymbol{\epsilon_\tau} = (\epsilon_\tau, \epsilon_\tau, ..., \epsilon_\tau), \boldsymbol{\epsilon_\tau} \sim \mathcal{N}(0, \tau) \quad (1)$$

Input	Description
TectonicRegionType	Tectonic region type [1]
Magnitude_Scaling_Relationship	Area-Magnitude Scaling Relationship [2]
Rupture_aratio	Rupture aspect ratio [3]
ID_Event	`Shakemap` ID of the event
Vs30file	$V_{S,30}$ filename
CorrelationModel	Correlation model [4]
CrosscorrModel	Croscorrelation model [5]
vs30_clustering	`True` if $V_{S,30}$ values show or are expected to show clustering [6]
truncation_level	Number of standard deviations for truncation of the crosscorrelation model distribution [7]

Table 1. Input information passed to the code. [1]As defined in the tectonic regionalisation of `OpenQuake`. [2]As defined in module `openquake.hazardlib.scalerel`. [3]As required from module `openquake.hazardlib.geo.surface.PlanarSurface.from_hypocenter` [4]As defined in module `openquake.hazardlib.correlation`. [5]As defined in module `openquake.hazardlib.cross_correlation`. [6]As required from module `openquake.hazardlib.correlation`. [7]As required from module `openquake.hazardlib.cross_correlation`.

$$\boldsymbol{\epsilon_\phi} = (\epsilon_{\phi_1}, \epsilon_{\phi_2}, ..., \epsilon_{\phi_S}), \boldsymbol{\epsilon_\phi} \sim \mathcal{N}(0, \Sigma) \tag{2}$$

with:

$$\Sigma = \begin{bmatrix} \phi_1^2 & \phi_1\phi_2\rho_{12} & \cdots & \phi_1\phi_S\rho_{1S} \\ \phi_2\phi_1\rho_{21} & \phi_2^2 & \cdots & \phi_2\phi_S\rho_{2S} \\ \vdots & \vdots & \ddots & \vdots \\ \phi_S\phi_1\rho_{S1} & \phi_S\phi_2\rho_{S2} & \cdots & \phi_1^S \end{bmatrix}$$

`ProbShakemap` relies on the `OpenQuake gmf` module to quantify the total GMMs uncertainty. For a given combination of rupture and GMM, the ground motion field (GMF) at each POI is simulated by sampling both $\boldsymbol{\epsilon_\tau}$ and $\boldsymbol{\epsilon_\phi}$, and adding them to $\boldsymbol{\mu}$ (Eq. (3)).

$$GMF = exp(\boldsymbol{\mu} + \boldsymbol{\epsilon_\tau} + \boldsymbol{\epsilon_\phi}) \tag{3}$$

Randomly sampling N times from the probability distributions of $\boldsymbol{\epsilon_\tau}$ and $\boldsymbol{\epsilon_\phi}$ returns a set of N ground motion fields. It is important to note that the returned GMF distribution is fixed for a given combination of source and POIs collection, thus assur-

ing the retrieval of the same set of ground motion fields each time the code is run. As the last step, predictions are aggregated at all the POIs, combining the GMFs sampled from the whole GMM set. Importantly, each GMM is sampled proportionally to its weight. In this way, the most relevant GMMs dominate the simulated GMFs. A more detailed description of the probabilistic analysis implemented in `ProbShakemap` is reported in Alg. 1.

Algorithm 1 Algorithm pseudocode for the probabilistic analysis implemented in `ProbShakemap`

Require:

- POIs file
- event.xml (`ShakeMap`-like)
- stationlist.json (`ShakeMap` output, only needed for data-based tools)
- $V_{S,30}$ file (optional)

STEP 1: Sampling Uncertainty
$K =$ number of scenarios in the ensemble
$G =$ number of GMMs
$S =$ number of POIs
$N =$ number of GMFs
for $k, scen\_k$ in ensemble **do**
    build `OpenQuake BaseRupture` object;
    build `OpenQuake` context object for the current combination of Source - `OpenQuake` Site Collection (= collection of POIs);
    compute means and standard deviations from the underlying GMMs.
    `// Statistical measures for a given combination of GMM and POI (the IM is fixed): mean,` σ `(Total Standard Deviation),` τ `( Inter-Event Standard Deviation),` ϕ `(Intra-Event Standard Deviation).`
    for g, GMM_g in GMM set **do**
        generate a distribution of n ground motion fields (GMFs), with $1 \leq n \leq N$ proportional to the weight of the current GMM.
        $\longrightarrow$ GMF array of shape (M, S, n), where M is the number of IMs ($M = 0$ as the IM is fixed in `ProbShakemap`).
    end for
end for
STEP 2: Aggregating Results
$\longrightarrow$ 3D matrix of shape (K, S, N) $\longrightarrow$ Ground-motion predictive distribution at each POI.
`// For each scenario, each POI is assigned the GMFs aggregated from all the GMMs.`

`ProbShakemap` offers a variety of functionalities: three utility tools (`StationRecords`, `Save_Output` and `QueryHDF5`) and three "prob tools": `GetStatistics`, `GetDistributions` and `EnsemblePlot`.

- `StationRecords`: inspects `Shakemap` .json station file and plots the recorded peak ground motions at the station locations.

- `Save_Output`: save the output of the probabilistic analysis to a .HDF5 file with the following hierarchical structure: scenario → POI → GMMs realizations.
- `QueryHDF5`: navigates and queries the .HDF5 file at a given scenario.
- `GetStatistics`: calculates and save the predictive distribution statistics at each POI; plots the results on a map.
- `EnsemblePlot`: visualizes and summarizes the key statistical features of the predictive distribution at the selected POIs with a boxplot.
- `GetDistributions`: plots the CDF of the predictive distribution at a specific POI together with the ground-motion value recorded either at the station coinciding with the POI or, if unavailable, at the nearest station (datum taken from the `Shakemap` .json station file). Importantly, this tool can be also used to associate an uncertainty interval to the peak ground motion recorded at a specific station.

The output of the probabilistic analysis described in Alg. 1 can be explored with any tool among `GetStatistics`, `GetDistributions` or `EnsemblePlot`.

2.2 ProbShakemap validation tests

We validate `ProbShakemap` against data by implementing the statistical test proposed in Selva et al. (2021b) for tsunami warning probabilistic forecasts. Here we only consider predictions at POIs coincident with stations. With this test, we verify the existence of significant biases in the forecasted peak ground motions. This is done by examining whether the differences between observed and expected values follow a distribution that includes the value 0, indicative of an unbiased forecast. We only consider stations located within a 100 km radius from the event epicenter, and recorded ground motions that are above a minimum threshold value of 0.1 cm/s^2 and 1 cm/s for PGA and PGV, respectively. We stack the misfit values calculated for all seismic stations, ensemble scenarios and GMMs realizations. Under the assumption that `ProbShakemap` predictions are unbiased, we expect the range 2.5 – 97.5 percentiles range to include the zero misfit.

In addition, we assess the predictive performance of `ProbShakemap` at all available stations located within a 100 km radius from the event epicenter. As for the bias test, we only consider recorded ground motions that are above a minimum threshold value of 0.1 cm/s^2 and 1 cm/s for PGA and PGV, respectively. Results are displayed using a traffic-light visualization system: if a ground-motion record falls within the 2.5^{th} - 97.5^{th} percentiles of the `ProbShakemap` predictive distribution at the corresponding station, it is represented by a green traffic light. Otherwise, it is shown as red.

3 Proof-of-concept

3.1 ProbShakemap for the 30 October 2016 Mw 6.5 Norcia earthquake

We first apply `ProbShakemap` to the 30 October 2016 Mw 6.5 Norcia earthquake, the largest among the three main shocks in the 2016 Amatrice-Visso-Norcia sequence. To account for site effects, we use the $V_{S,30}$ dataset included in the `ShakeMap`

Italian configuration, which implements the $V_{S,30}$ model compiled by Michelini et al. (2020) for the Italian region. The list of POIs consists of 1,552 geographical points, including the 472 seismic stations listed in `ShakeMap stationlist.json` file and the 1,080 nodes of a $\approx 10-km$ spaced grid ($400km$ x $270km$) centered at the event epicenter. The first step consists of running `SeisEnsMan` to generate the ensemble of source scenarios (for more details on the scenarios sampling, see Section 2). After testing various ensemble sizes, we found that an ensemble of 1,000 scenarios effectively captures the source uncertainty for this particular event. Fig. S1 in the Supplementary Material shows the range of source parameters sampled from the 1,000 scenarios in the ensemble. As Intensity Measure (IM), we consider PGA (g) and PGV (cm/s). In the Italian implementation of ShakeMap, only one GMM is adopted for the area struck by the Mw 6.5 Norcia earthquake occurred (Bindi et al., 2011). For each scenario in the ensemble, we sample this GMM a total of 10 times, resulting in 10,000 (K x N, i.e. 1,000 x 10) PGA/PGV values predicted at each POI. For the application presented here, we only show the results for PGA and PGV, although `ProbShakemap` is capable of performing the analysis for SA(0.3), SA(1.0), SA(3.0) as well. Nonetheless, similar conclusions can be drawn for these spectral values.

The main output of `ProbShakemap` consists of various products for inspecting and visualising the distribution of ground-motion predictions at the POIs (or at a subset of POIs). In the following, we present products related to PGA (the PGV output can be found in Fig. S2-S4 of the Supplementary Material).

Fig. 1 is the output of the module `GetStatistics`, i.e. the statistics summarizing the PGA predictive distribution at each POI of the $\approx 10-km$ grid (stations have been excluded for visualization purposes). The output shows significant spatial variability in ground motion. Peaks of ground motion align along the NW-SE direction, consistent with the prevailing fault striking in that portion of the Apennines. Considering the maps at the 10^{th} and 90^{th} percentiles, we find that the region experiencing the highest ground shaking covers an area of approximately 100 km^2, with a maximum value of approximately $0.3g$ in the 10^{th} percentile map. In the 90^{th} percentile map, locations experiencing a PGA $\geq 0.1g$ cover most of the grid, whereas near the epicenter PGA values exceed $0.5g$.

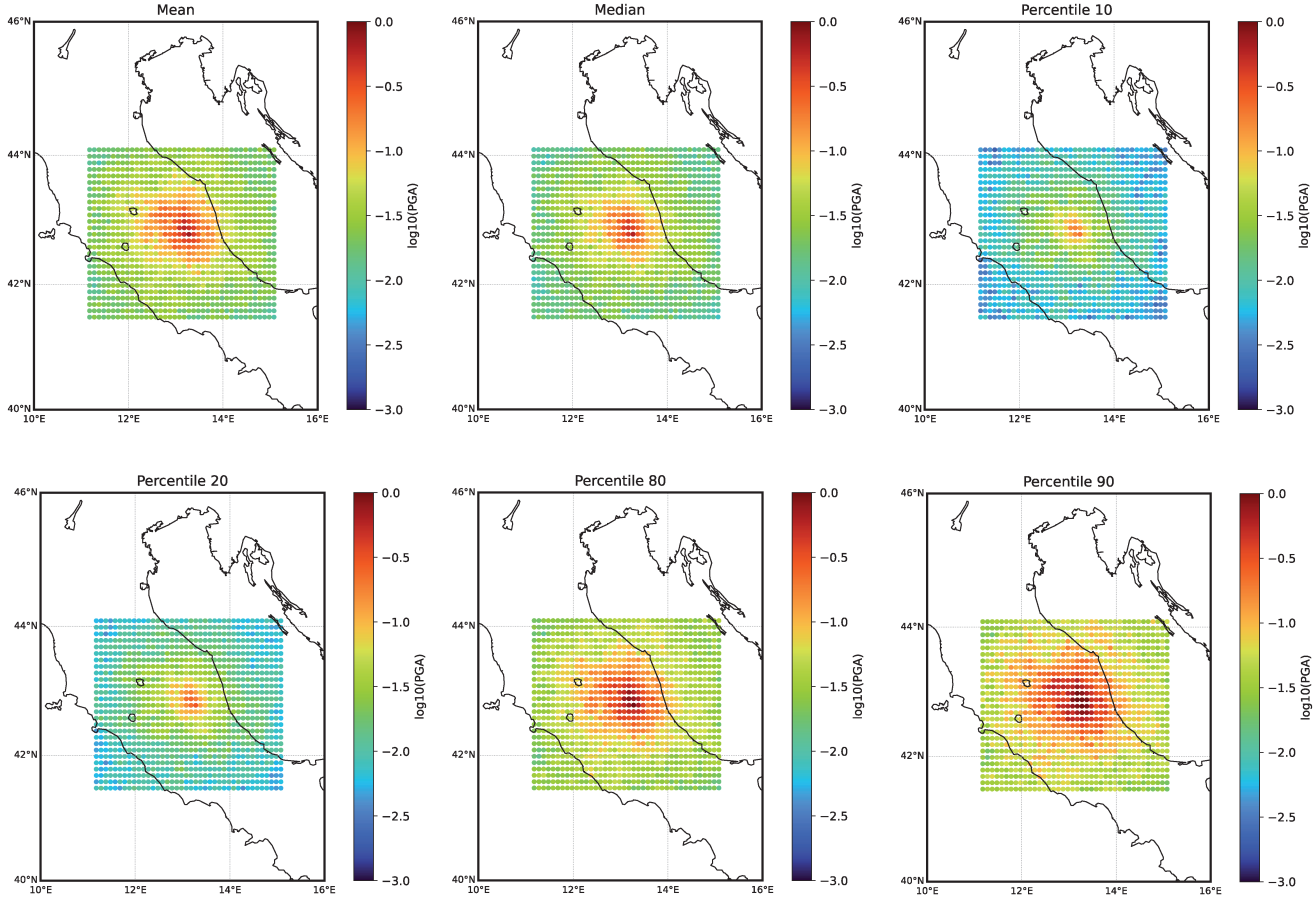

Figure 1. `GetStatistics` output for the 30 October 2016 Mw 6.5 Norcia earthquake: mean, median, percentile 10, percentile 20, percentile 80, percentile 90 of the distribution of 10,000 (1,000 x 10) $\log PGA$ values (g) at each POI of the regular grid. Stations have been ignored for visualization purposes and to align with the standard `ShakeMap` layout.

To focus our analysis on specific POIs, we use the options `pois_subset` and `pois_selection_method` of `ProbShakemap` to extract a set of 20 azimuthally uniformly distributed POIs at a maximum distance of 50 ± 5km from the epicenter. The selected subset is shown in Fig. 2a. To explore the variability of the predicted ground-motions across the selected POIs, we implement the `EnsemblePlot` module to visualize the key statistical features of the predictive distribution at each of the selected POIs (Fig. 2b). We notice that the POIs exhibiting the highest variability in the predictive distribution are POIs 7, 8 and 9, which are all clustered on the N-W section of the fault area. This may suggest a greater likelihood of relatively higher ground-motion values within the N-W section of the fault area compared to other regions of interest. It could also imply a larger indeterminacy in estimating the ground motion for POIs located along directions nearly coinciding with the fault strike.

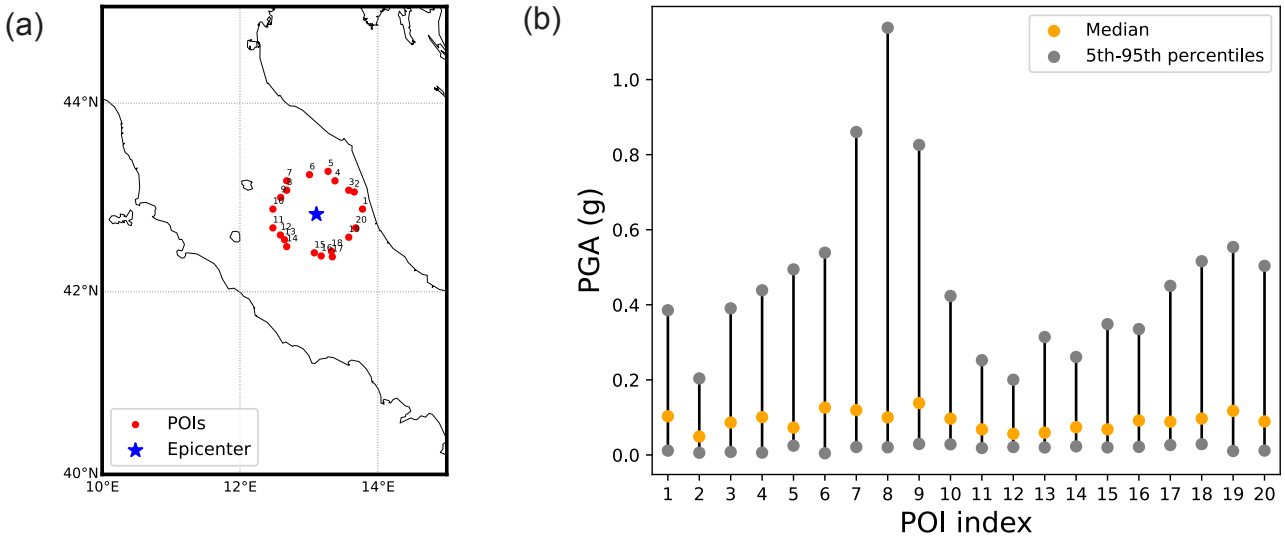

Figure 2. (a) Map of the POIs subset extracted by `ProbShakemap`. POIs are selected to be evenly distributed with respect to the azimuth and to lie within a ring at a distance of $50 \pm 5km$ from the event epicenter. (b) `EnsemblePlot` output for the 30 October 2016 Mw 6.5 Norcia earthquake summarizing the PGA (g) predictive distribution at each POI of the subset with median and 5^{th} and 95^{th} percentiles.

We then use the `GetDistributions` module to compare the PGA predictive distribution at the set of POIs with the PGA value recorded at the corresponding stations, if available, or at the nearest stations. The PGA distribution is summarized with the Cumulative Distribution Function (CDF) and three main statistics: median, 10^{th} and 90^{th} percentiles. For visualization purposes, Fig. 3 shows the output for only 4 of the 20 POIs, all coinciding with stations. Fig. S5 in the Supplementary Material presents the output for all 20 POIs, and shows that the PGA recorded values fall in the range 10^{th} - 90^{th} percentiles at all POIs except two.

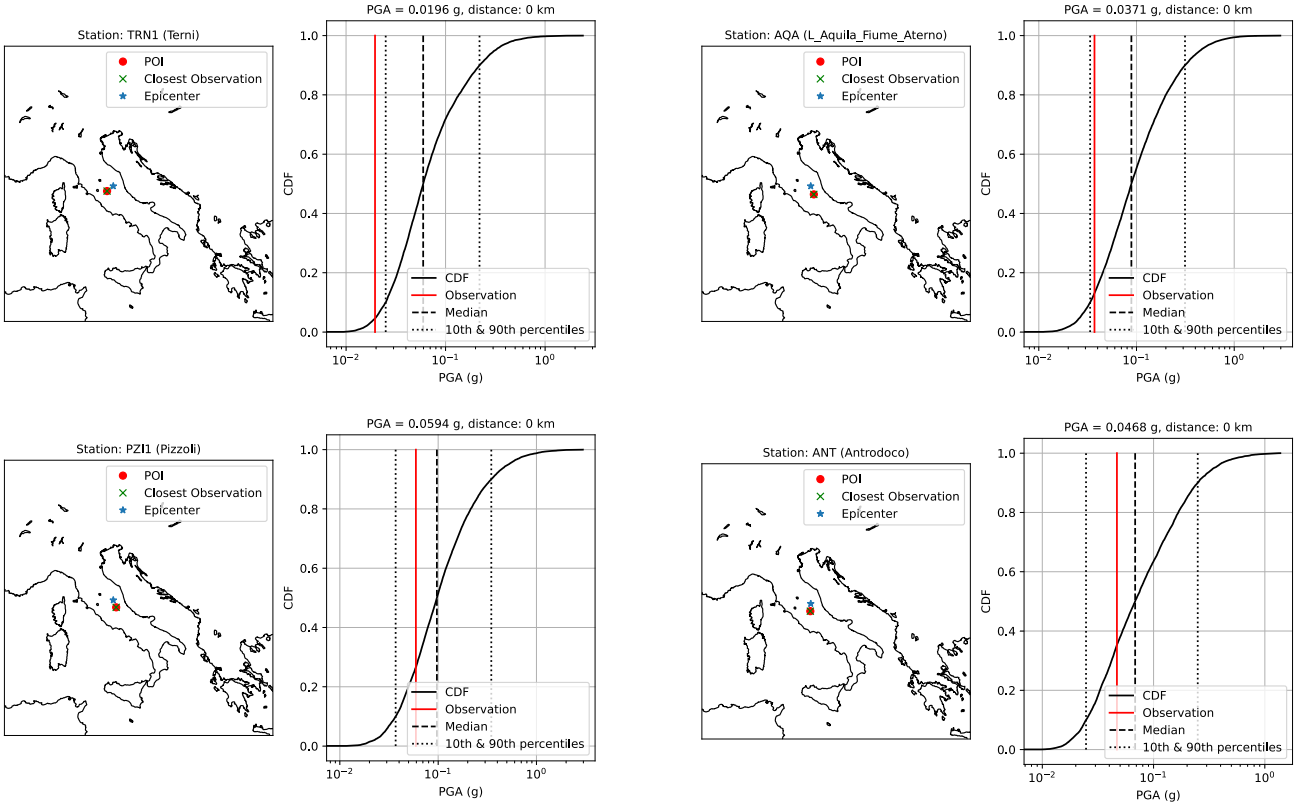

Figure 3. `GetDistributions` output for the 30 October 2016 Mw 6.5 Norcia earthquake (at 4 of the 20 POIs plotted in Fig. 2a, all co-located with stations): PGA (g) recorded values are compared with the PGA predictive distribution at each POI. On the left-hand side of each plot, a map shows the epicenter location, the selected POI and the position of the station. On the right-hand side, the CDF of the PGA predictive distribution is plotted with highlighted the main statistics: median, 10^{th} and 90^{th} percentiles. The red line corresponds to the datum value. On top, the PGA recorded value is shown together with the POI-station distance.

To assess the accuracy of our predictions to account for the spatial correlation of ground motions correctly, we implement a bias test similar to the one adopted in Selva et al. (2021b) (see Section 2.2 for more details on this test). Our expectation is that the distribution of these misfits will not deviate significantly from zero (further details are available in Section 2). We have identified 147 (131) stations within 100 km radius from the event epicenter where PGA (PGV) is $\geq 0.1cm/s^2$ ($\geq 1cm/s$).

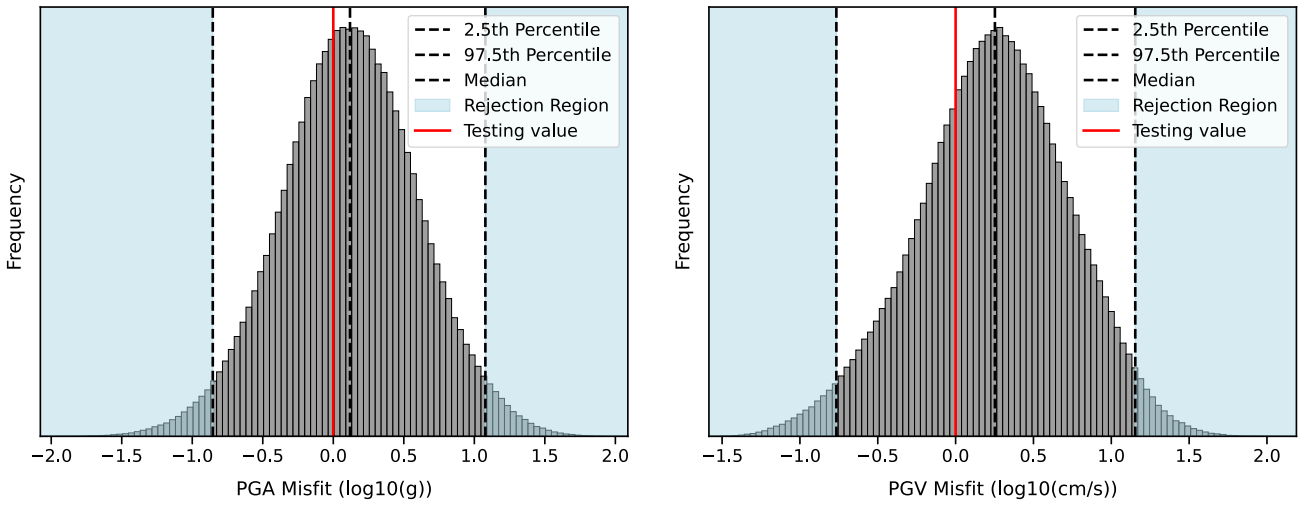

Figure 4. Bias test for the 30 October 2016 Mw 6.5 Norcia earthquake. Left: PGA (log10(g)), Right: PGV (log10(cm/s)). The red dashed line is the testing value (zero misfit), whereas the three dashed lines are the 2.5 percentile, the median and the 97.5 percentile. The test is rejected (i.e., predictions are biased) if the testing value falls in the rejection region, whereas it is accepted if the testing value falls within the 95% confidence interval.

The results of the bias test are shown in Fig. 4. We observe that predictions are overall accurate, meaning that the spatial correlation of ground motion is correctly reproduced. We additionally test the predictive performance of `ProbShakemap` using the traffic-light method described in Section 2. Results are shown in Fig. 5. We observe that `ProbShakemap` can predict data with a 95% confidence level at the majority of the stations.

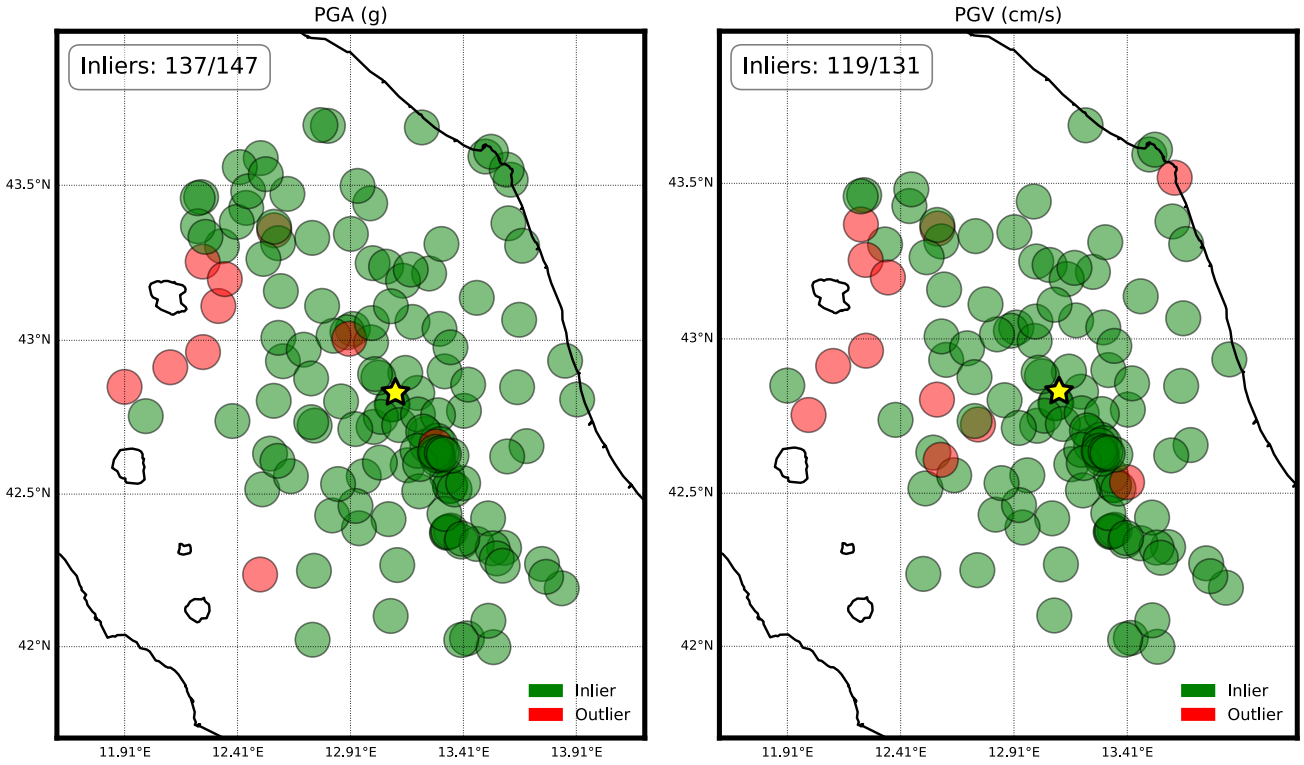

Figure 5. Traffic-light visualization of `ProbShakemap` performance against data (for stations at a distance less than 100 km from the event epicenter). If a ground-motion record falls within the 2.5^{th} - 97.5^{th} percentiles of the `ProbShakemap` predictive distribution at the station, it is represented by a green traffic light (inlier). Otherwise, it is shown as red (outlier). The yellow star indicates the event epicenter. Left: PGA (g) results; Right: PGV (cm/s) results.

3.2 ProbShakemap for the 6 February 2023 Mw 7.8 Pazarcik earthquake

Here we apply `ProbShakemap` to the 6 February 2023 Mw 7.8 Pazarcik earthquake, which is part of the Kahramanmaraş Mw 7.8-7.6 earthquake doublet sequence that ruptured at least six major fault segments of the East Anatolian Fault system (Jia et al., 2023). The list of POIs comprises 500 nodes of a $\approx 20 - km$ spaced regular grid ($500km$ x $400km$) centered at the event epicenter. The ensemble includes 1,000 earthquake source scenarios. Fig. S6 in the Supplementary Material shows the distribution of source parameters from the 1,000 scenarios in the ensemble. We consider only PGA as IM since not all the GMMs available for this area include PGV. The GMMs retrieved by `ProbShakemap` for this event are: AkkarEtAlRjb2014 (Akkar et al., 2014), AbrahamsonEtAl2014 (Abrahamson et al., 2014), BooreEtAl2014LowQ (Boore et al., 2014), Campbell-Bozorgnia2014LowQ (Campbell and Bozorgnia, 2014), CauzziEtAl2014 (Cauzzi et al., 2015), ChiouYoungs2014 (Chiou and Youngs, 2014), ZhaoEtAl2016Asc (Zhao et al., 2016). These GMMs have been sampled 7, 7, 1, 1, 1, 1, 2 times over a total of 20 times, respectively. For this event, we use $V_{S,30}$ default values (760 m/s).

Fig. 6 summarizes the PGA predictive distribution at each POI of the regular grid with basic statistics. Compared to the Mw 6.5 Norcia earthquake, where the highest PGA values are expected to concentrate near the event epicenter, for the Mw 7.8 Pazarcik earthquake `ProbShakemap` predicts relatively high PGA values on a much wider area surrounding the epicenter, as expected. The 10^{th} and 90^{th} percentile map predicts a PGA value of about $0.03g$ and $\geq 0.3g$, respectively, at the majority of POIs.

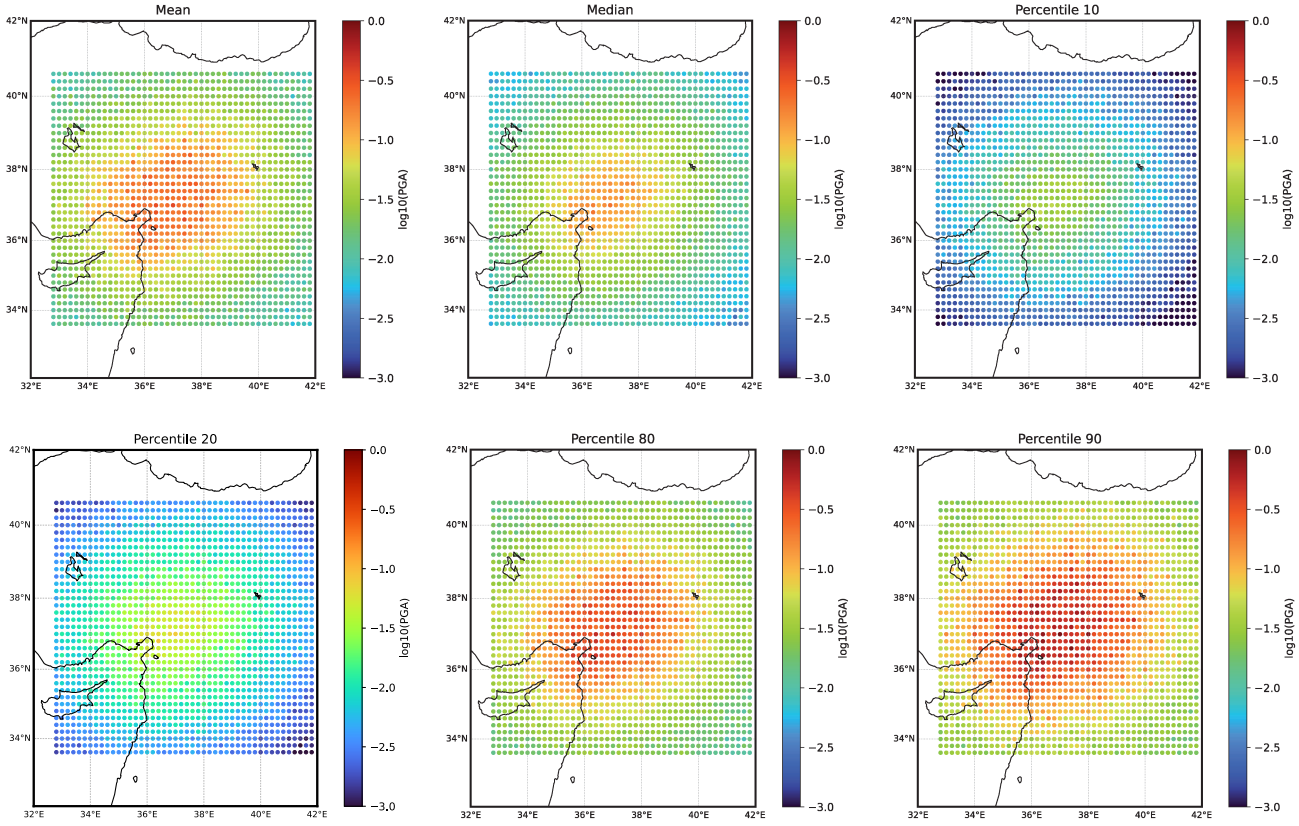

Figure 6. `GetStatistics` output for the 6 February 2023 Mw 7.8 Pazarcik earthquake: mean, median, percentile 10, percentile 20, percentile 80, percentile 90 of the distribution of 20,000 (1,000 x 20) PGA (g) values at each POI of the regular grid.

Following the previous proof of concept, we select 20 azimuthally uniformly distributed POIs at a maximum distance of $100km$ from the event epicenter. Fig. 7a shows the selected POIs as returned by `ProbShakemap`. Fig. 7b explores the predictive distribution variability across the POIs' subset. In contrast to the Mw 6.5 Norcia earthquake, we do not notice any azimuth-dependent pattern in the expected uncertainty. However, we notice that at POI 5, situated to the north-northeast of the event epicenter, `ProbShakemap` predicts a substantially higher variability in ground-motion values.

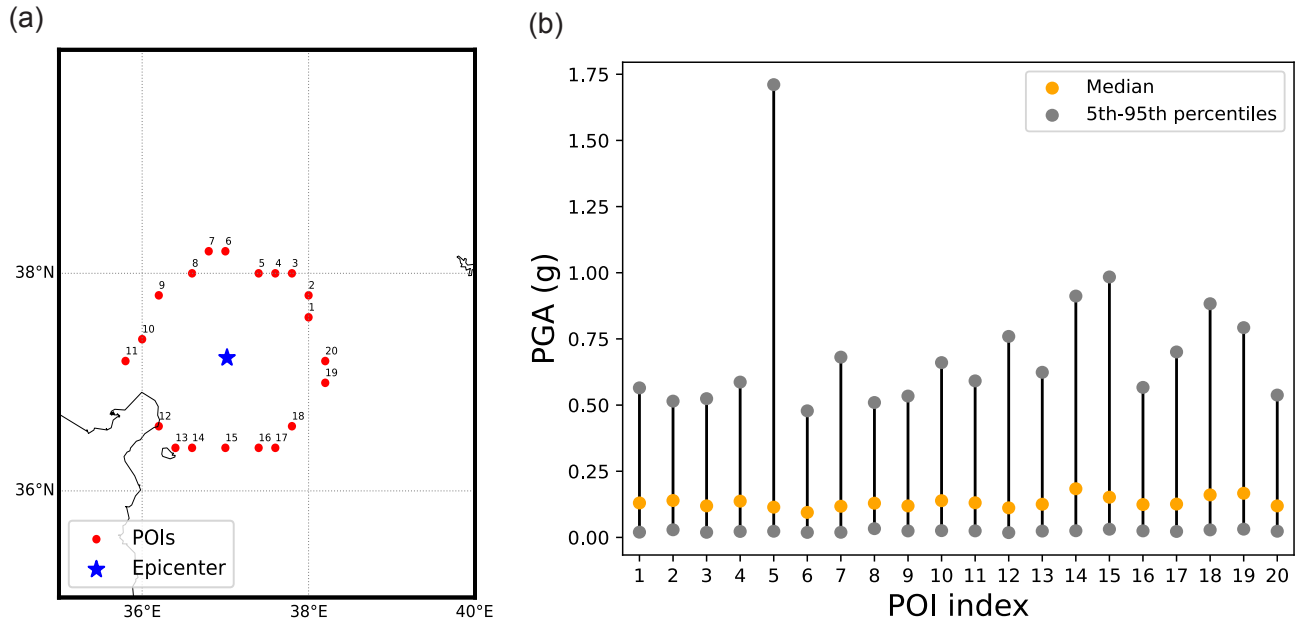

Figure 7. (a) Map of the POIs subset as returned by `ProbShakemap`. POIs are selected to be evenly distributed with respect to the azimuth and to lie within a ring at a distance of $100 \pm 10km$ from the 6 February 2023 Mw 7.8 Pazarcik earthquake epicenter. (b) `EnsemblePlot` output for the 6 February 2023 Mw 7.8 Pazarcik earthquake summarizing the PGA (g) predictive distribution at each POI of the subset with median and 5^{th} and 95^{th} percentiles.

Fig. S7 displays the primary tectonic features of the East Anatolian Zone, with highlighted the Mw 7.8-7.6 earthquake doublet and the Mw 4+ earthquakes occurred in the following 10 days. We recall here that only the Mw 7.8 Pazarcik earthquake, i.e. the first earthquake of the doublet, served as an input event for the `ProbShakemap` analysis. Notably, POI 5 sits along one of the fault segments that ruptured during the doublet sequence, in the proximity of a triple junction. Here `ProbShakemap` predictive distribution exhibits the largest uncertainty among all POIs.

Finally, we compare the PGA predictive distribution at the selected POIs with the PGA value recorded at the closest station. We recall that, differently from the previous proof-of-concept, here we are considering a regular grid as input, which does not include POIs coinciding with stations. Fig. 8 shows the output for 4 POIs only. Results for all the 20 POIs can be visualized in Fig. S8 of the Supplementary Material. The latter shows that the PGA recorded values fall in the range 10^{th} - 90^{th} percentiles for all the POIs except for 3, even if POIs are not coinciding with stations. To validate `ProbShakeMap` against data, we re-run the probabilistic analysis, this time using as input POIs file a combination of the $500km$ x $400km$ regular grid and the stations' locations.

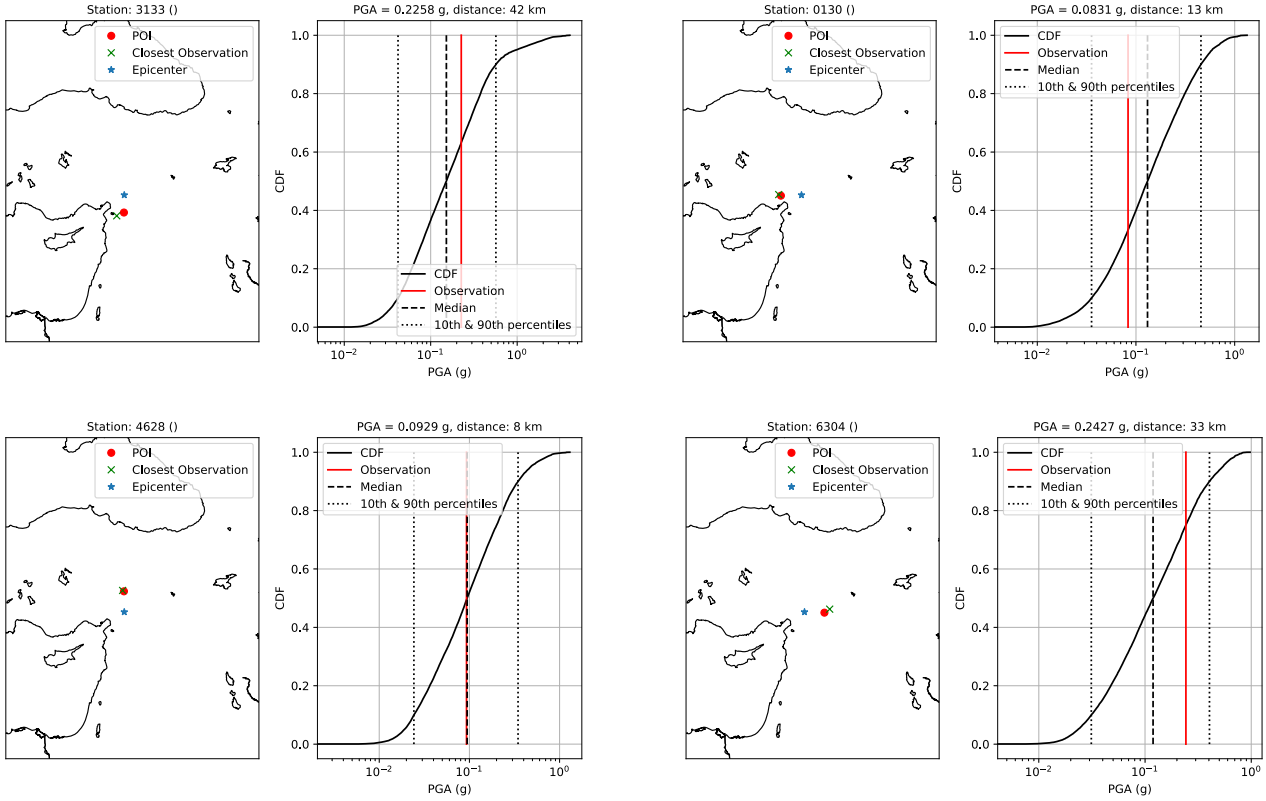

Figure 8. `GetDistributions` output for the 6 February 2023 Mw 7.8 Pazarcik earthquake (at only 4 of the 20 POIs plotted in Fig. 7a): PGA (g) recorded values are compared with the PGA predictive distribution at each POI. On the left-hand side of each plot, a map shows the epicenter location, the selected POI and the position of the closest station. On the right-hand side, the CDF of the PGA predictive distribution is plotted with highlighted the main statistics: median, 10^{th} and 90^{th} percentiles. The red line corresponds to the datum value. On top, the PGA recorded value is shown together with the POI-station distance.

We then employ the bias test introduced for the Mw 6.5 Norcia earthquake. There are 31 stations within a 100 km radius from the event epicenter where PGA is $\geq 0.1 cm/s^2$. Results are shown in Fig. 9. For this case as well, our predictions are accurate overall.

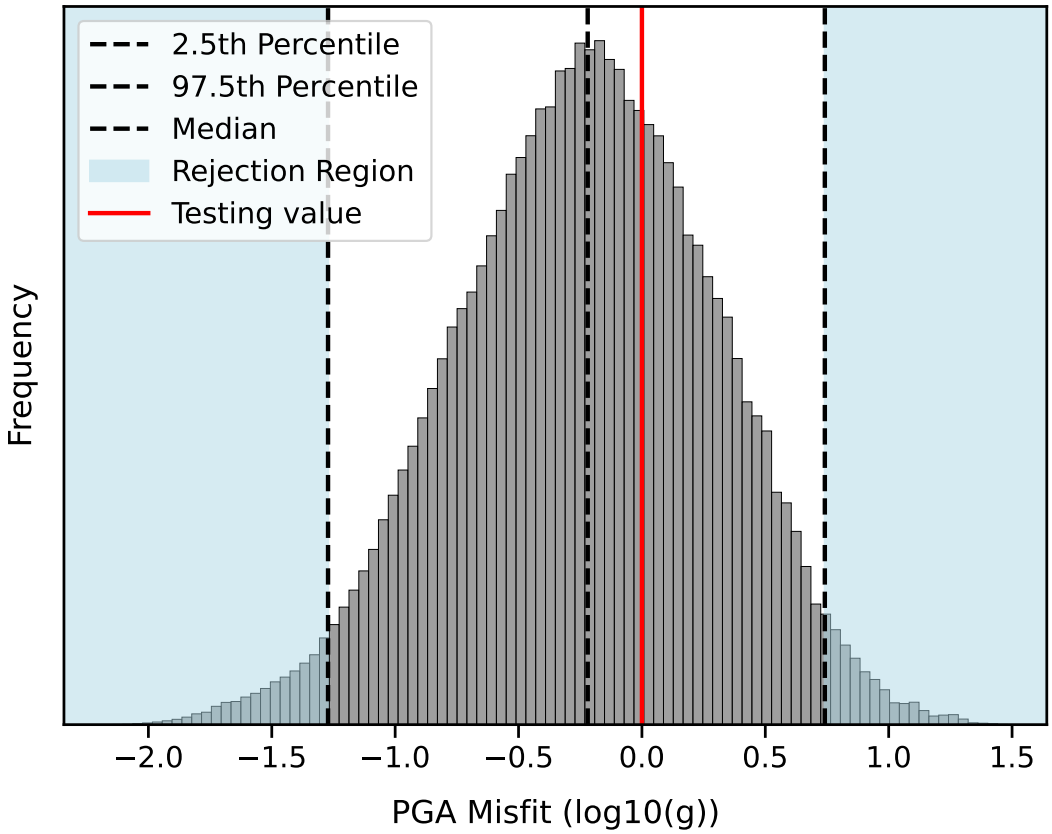

Figure 9. Bias test for the 6 February 2023 Mw 7.8 Pazarcik earthquake (PGA only (log10(g))). The red dashed line is the testing value (zero misfit), whereas the three dashed lines are the 2.5 percentile, the median and the 97.5 percentile. The test is rejected (ie. predictions are biased) if the testing value falls in the rejection region, whereas it is accepted if the testing value falls within the 95% confidence interval.

Results from the traffic-light method described in Section 2 are shown in Fig. 10. Once again, we find that `ProbShakemap` can predict data with a 95% confidence level at the majority of the stations.

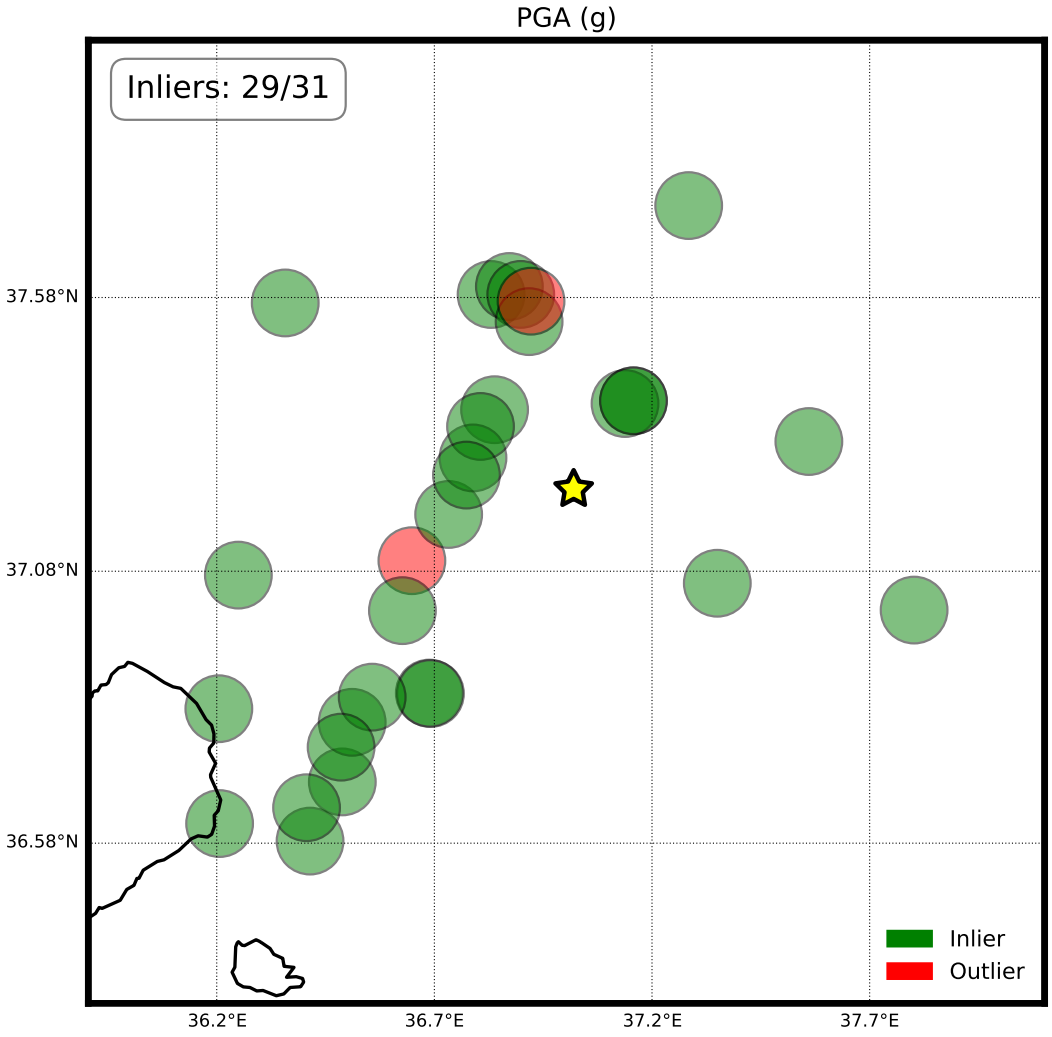

Figure 10. Traffic-light visualization of `ProbShakemap` performance against data (for stations at a distance less than 100 km from the event epicenter). If a ground-motion PGA record (g) falls within the 2.5^{th} - 97.5^{th} percentiles of the `ProbShakemap` predictive distribution at the station, it is represented by a green traffic light (inlier). Otherwise, it is shown as red (outlier). The yellow star indicates the event epicenter.

3.3 `ProbShakeMap` vs `ShakeMap`

The USGS `ShakeMap` software provides uncertainty estimates in the form of a grid file containing medians and standard deviations for all ground-motion parameters at each grid point. While the seismic source is assumed to be known, the GMMs uncertainty is quantified by combining two terms: 1) intra-event variability: spatial variability of strong-motion data error controlled by the record proximity to the seismic stations (where it reduces to zero if the station lies on the `ShakeMap` grid); 2) inter-event variability: GMM variability within the frame of multivariate normal distribution (Worden et al., 2018; Engler

et al., 2022). In ProbShakeMap, the GMMs uncertainty is modelled as in ShakeMap. In addition to that, ProbShakeMap accounts for earthquake source uncertainty by computing ensemble-based forecasts capturing the variability in source parameters.

Here we compare ShakeMap and ProbShakemap predictions at 12 random POIs for the Mw 6.5 Norcia earthquake (see Fig. 11). The selection of the 12 POIs was constrained by their inclusion in both the ShakeMap and ProbShakemap grids. Since ProbShakemap samples the total GMMs variability as in ShakeMap, and considering that the input $V_{S,30}$ file (i.e., the $V_{S,30}$ model adopted by Michelini et al., 2020) is consistent between both software, the differences observed in distributions between ProbShakemap and ShakeMap at the specified POIs can be attributed to two factors: the incorporation of real data in ShakeMap and/or the quantification of the source effect implemented in ProbShakemap. In the context of this test, the 12 POIs were selected with a maximum distance of $100km$ from the hypocentre, to specifically highlight the discrepancies due to the influence of source uncertainties.

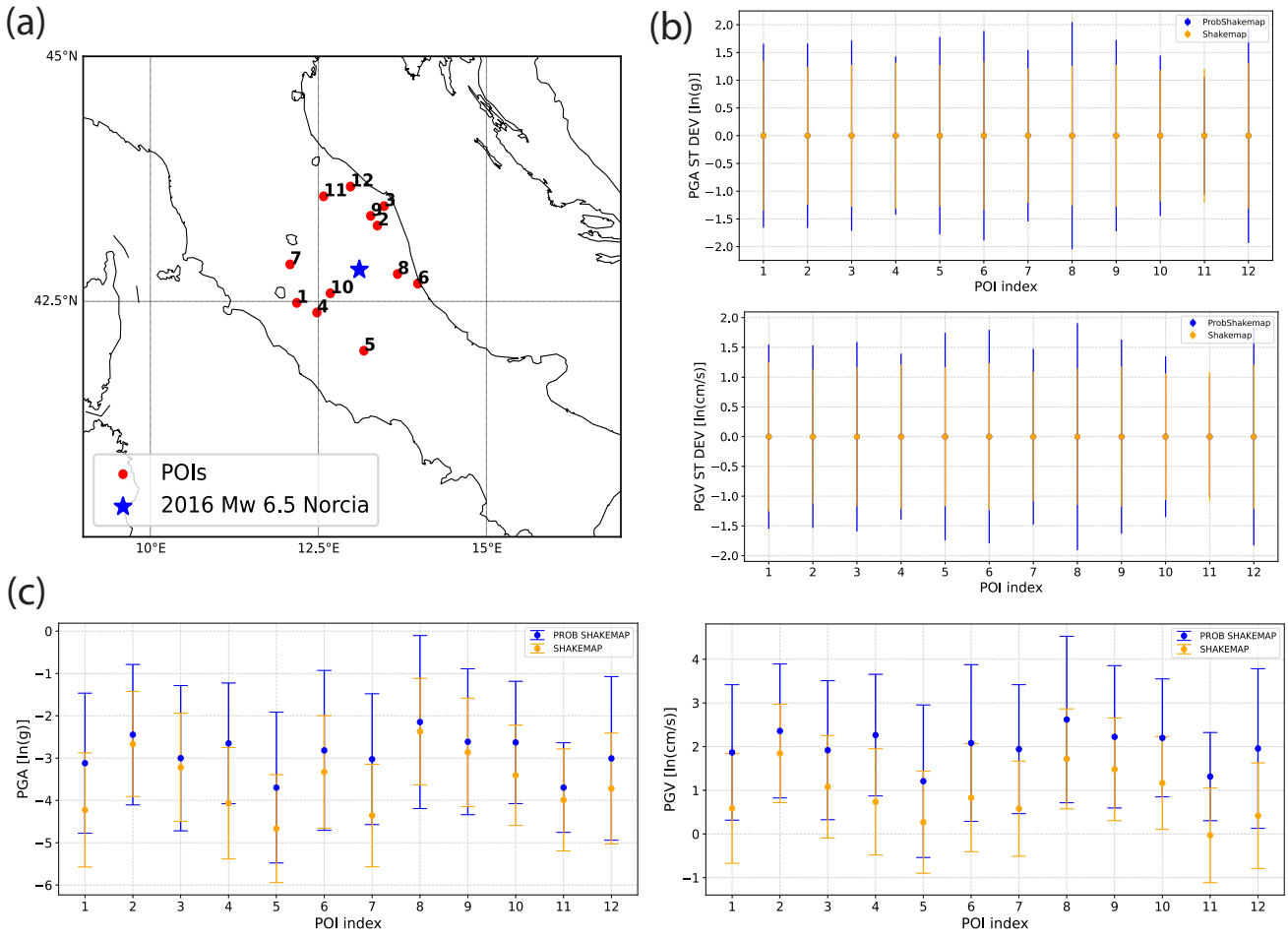

Figure 11. Output comparison between USGS `ShakeMap` software and `ProbShakemap` at 12 randomly distributed POIs. a) Map of the POIs; b) 2σ for `ProbShakemap` (blue) and `ShakeMap` (orange) distributions (in logarithmic scale) for PGA (top) and PGV (bottom); c) Median $\pm 2\sigma$ for the `ProbShakemap` (blue) and `ShakeMap` (orange) distributions (in logarithmic scale) for PGA (left) and PGV (right).

Fig. 11 presents a comparison of 2σ (Fig. 11b) and medians $\pm 2\sigma$ (Fig. 11c). As expected, `ProbShakemap` exhibits consistently higher variability in ground-motion predictions compared to `ShakeMap`, although this discrepancy is not spatially uniform. At some POIs (e.g., POIs 8,12), it increases, whereas at other POIs (e.g., POI 4,11), the two distributions compare better. Such variability, which the GMMs alone may not fully account for, could be attributed to the combined influence of source characteristics and local site conditions on overall uncertainty estimation. Notably, `ProbShakemap` median is substantially higher than the `Shakemap` median at all POIs. This implies that, for the Norcia earthquake, `ProbShakemap` predictive distributions tend to be shifted towards higher values of PGA/PGV.

We perform the same analysis for the 2023 Mw 7.8 Pazarcik earthquake (Fig. 12). The 12 POIs have been selected within $200km$ from the hypocentre. In this case, `ProbShakemap` and `ShakeMap` distributions exhibit a greater discrepancy com-

pared to the Norcia earthquake. However, ProbShakemap predictive distributions are not always shifted towards higher values.

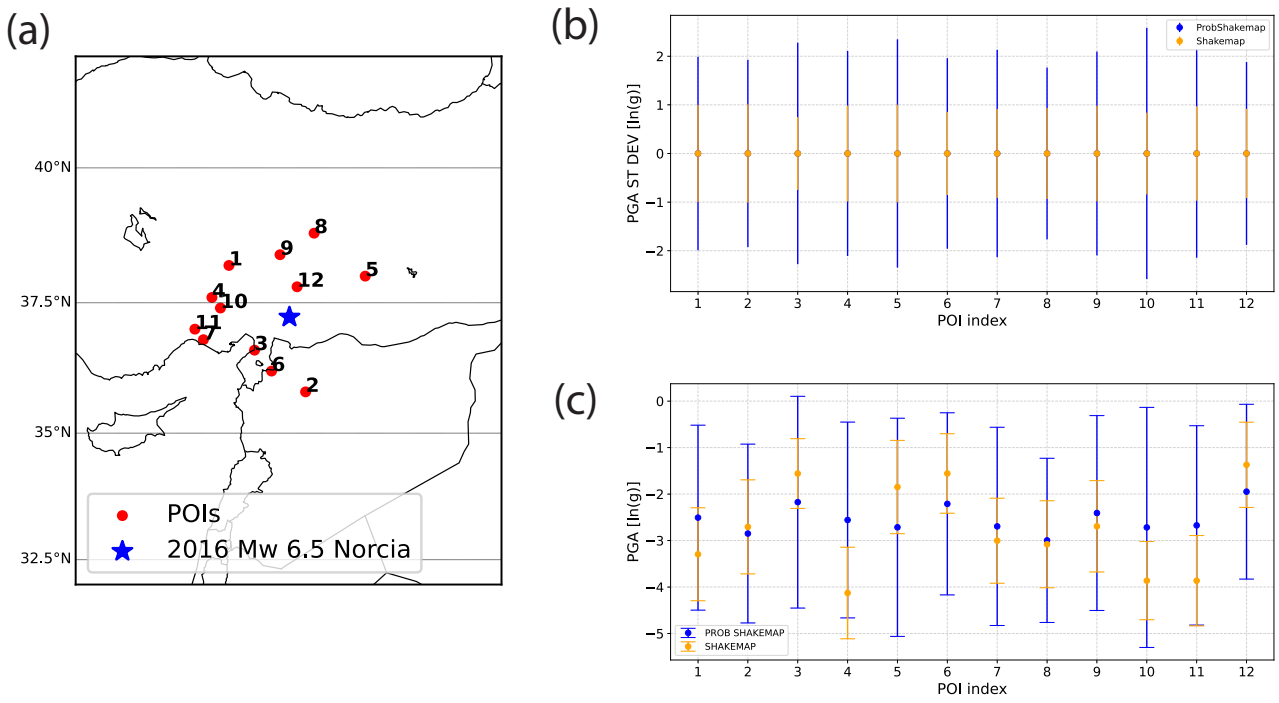

Figure 12. Output comparison between USGS ShakeMap software and ProbShakemap at 12 randomly distributed POIs. a) Map of the POIs; b) 2σ for ProbShakemap (blue) and ShakeMap (orange) distributions (in logarithmic scale); c) Median $\pm 2\sigma$ for ProbShakemap (blue) and ShakeMap (orange) distributions (in logarithmic scale).

We here stress that ShakeMap is an evolving product and that the initial maps, containing only the epicenter and data, are available within a few minutes after a strong earthquake occurs. For larger events, requiring the definition of the extended source and the inclusion of source geometry, this can take several hours. Conversely, ProbShakeMap relies solely on the input of hypocenter and magnitude estimations, accessible within seconds to minutes after the event.

4 Discussion and Conclusion

Uncertainty quantification plays a pivotal role in forecasting nonlinear processes, serving the purpose of quantifying both our lack of knowledge about the process (epistemic uncertainty) and its inherent randomness (aleatoric uncertainty). This task is particularly challenging in the context of UC, where information and its uncertainty must be released within minutes to hours following an earthquake. Physics-based simulations of multiple ground-motion scenarios would represent the most accurate

290 solution for quantifying the uncertainty on the peak ground shaking expected at a given grid of points. But, even with significant advancements in HPC systems, full-ensemble physics-based simulations are not tractable on a time scale of minutes to hours.

Here we have presented `ProbShakemap`, a Python toolbox designed to address earthquake source uncertainty quantification in UC applications. It generates an ensemble of event-compatible scenarios capturing source uncertainty and implements GMMs to propagate source uncertainty to peak ground-motion estimates (PGA, PGV, SA(0.3), SA(1.0), SA(3.0)) at spe-
295 cific points of interest. `ProbShakemap` also quantifies model uncertainty by sampling all available GMMs for the region and the GMMs inherent variability. The predictive distribution of ground motion values at the grid of POIs can be explored both visually and quantitatively through the `ProbShakemap` "prob tools": `GetStatistics`, `GetDistributions` and `EnsemblePlot`.

In this paper, we have shown the capabilities of `ProbShakemap` through two proof-of-concept examples — the 30 October
300 2016 Mw 6.5 Norcia earthquake and the 6 February 2023 Mw 7.8 Pazarcik earthquake. As an illustration of `ProbShakemap` computational performance, we consider its first proof-of-concept, where we examined 1,000 earthquake source scenarios and 1,552 POIs: notably, all three different products of `ProbShakemap` (Fig. 1, Fig. 2, Fig. 3) were generated in approximately 10 minutes using a standard laptop equipped with 8 CPUs. This outcome highlights `ProbShakemap`'s potential in addressing the critical period between the event occurrence time and the retrieval of initial estimates of source geometry parameters. Without
305 relying on source inversion completion, in a few minutes `ProbShakemap` computes ground-motion predictive distributions encompassing both source and GMMs uncertainty. Yet, significant source uncertainty persists even after retrieving the initial source parameters. For this reason, the implementation of `ProbShakemap` based on subsequent updates of the scenario ensemble holds promise for uncertainty quantification also after first estimates of source parameters become available (see Section 5).

310 Besides its role in uncertainty quantification for UC applications, `ProbShakemap` provides valuable additional insights. For the Norcia proof-of-concept, we showed that the distribution of peak ground-motion values displays greater variability along the N-W section of the fault area. In this case, the POIs are located outside the finite fault, also striking NW. This outcome implies that, given the provided ensemble of 1,000 scenarios resembling long-term source uncertainty and the GMM available for the region (Bindi et al., 2011), relatively higher peak ground-motion values and larger uncertainties can be expected in the
315 N-W section of the fault area. We observed something similar in the second proof of concept at POI 5, located at the triple junction of the East Anatolian Fault system. We believe that local seismotectonics, which are accounted for when sampling the fault geometry parameters of the ensemble scenarios, could be responsible for larger uncertainties at specific locations compared to others. The GMMs alone cannot account for these uncertainties. The two proofs-of-concept also highlighted the effect of incorporating earthquake source uncertainty on the characteristics of the final predictive distribution. When an
320 ensemble of plausible source scenarios is included in the analysis, the predictive distribution of ground motion can be shifted towards higher values (Norcia earthquake) or exhibits a substantially higher uncertainty (Pazarcik earthquake) with respect to `Shakemap` predictions. This comparative test demonstrates that there is no unique answer to how the output of the two software compares. `ProbShakemap` is a probabilistic tool that accounts for historical seismic activity and known faults, and it is independent of data. The extent to which its predictive distributions align with data-based `ShakeMap` predictions depends

on the capability of the ensemble to capture the whole source uncertainty and on the relative likelihood of the event with respect to the remaining scenarios in the ensemble.

Another useful resource provided by `ProbShakemap` is the `GetDistributions` tool (cf. Fig. 3 and Fig. 8), which enables the association of an uncertainty range to ground-motion recorded at seismic stations. This practice can be a valuable standard, especially in areas where little or no data are available since it can contribute to providing a more comprehensive and precise representation of potential ground motions at specific locations.

Lastly, we want to emphasize the implications of `ProbShakemap` being independent of any recorded data, with the exception of the magnitude and hypocenter estimates that are available within minutes after the occurrence of any event worldwide. Our analysis has evidenced that in cases where recorded ground motion data is accessible, the majority of the ground motion recorded values fall within the 2.5^{th} - 97.5^{th} percentiles interval of the predictive distribution (Fig. 5 and Fig. 10). This finding suggests that `ProbShakemap` can be utilized to generate estimates of peak ground shaking and their associated uncertainties in regions where recorded data may be lacking. The resulting ground motion distributions can then be integrated with knowledge about the vulnerabilities present in the affected areas, enabling the generation of impact assessments, an essential element for disaster risk managers and civil protection authorities.

5 Future developments

We aim to automate the update of the ensemble scenarios probabilities used in `ProbShakemap`. In the context of UC applications, this aspect is crucial, given that uncertainty about the source decreases as new information becomes available. To address this, `ProbShakemap` will dynamically adjust ensemble scenario probabilities, refining ground motion predictions at the POIs. A similar approach has already been developed for tsunami UC workflows (Cordrie et al., 2023).

Code and data availability. `ProbShakemap` is a stand-alone open-source software, available on GitHub (https://github.com/INGV/ProbShakemap) and Zenodo (https://doi.org/10.5281/zenodo.10654186). In the context of the European project eflows4HPC (https://eflows4hpc.eu/urgent-computing/), it will be integrated within UCIS4EQ (Urgent Computing Integrated Services for EarthQuakes), a HPC-based urgent seismic simulation workflow for physics-based short-time probabilistic forecast of an earthquake's impact (de la Puente et al., 2020). Regarding the 30 October 2016 Mw 6.5 Norcia earthquake, `ShakeMap` products (`stationlist.json`, `uncertainty.xml`, and `grid.xml`) were downloaded from http://shakemap.ingv.it/shake4/downloadPage.html?eventid=8863681. Similarly, for the 6 February 2023 Mw 7.8 Pazarcik earthquake, the corresponding `ShakeMap` products were downloaded from http://shakemapeu.ingv.it/downloadPage.html?eventid=20230206_0000008. `ProbShakemap` relies on the INGV `shakemap4` configuration, available via Docker at https://github.com/INGV/shakemap/releases/tag/v4.1.3.

Author contributions. AS contributed to the conceptualization of the methodology and `ProbShakemap`, developed the algorithm, and wrote the article. JS contributed to the conceptualization of the methodology, wrote the `GetStatistics` tool, and reviewed the manuscript.

LC authored the `SeisEnsMan` tool, tested `ProbShakemap` on the INGV-Bologna ADA cluster, and contributed to the manuscript review. LF and AM contributed to the validation of `ProbShakemap` against `Shakemap` and to the manuscript review. VL tested and developed the INGV Shakemap Docker and provided the technical support.

Competing interests. The contact author has declared that none of the authors has any competing interests.

Acknowledgements. This research was funded by the European High-Performance Computing Joint Undertaking (JU) under grant agreement No 955558 (eFlows4HPC, https://eflows4hpc.eu/urgent-computing/).

.

References

Abrahamson, N. A., Silva, W. J., and Kamai, R.: Summary of the ASK14 ground motion relation for active crustal regions, Earthquake Spectra, 30, 1025–1055, 2014.

Akkar, S., Sandıkkaya, M. A., and Bommer, J. J.: Empirical ground-motion models for point-and extended-source crustal earthquake scenarios in Europe and the Middle East, Bulletin of earthquake engineering, 12, 359–387, 2014.

Anderson, J. G. and Brune, J. N.: Probabilistic seismic hazard analysis without the ergodic assumption, Seismological Research Letters, 70, 19–28, 1999.

Atik, L. A., Abrahamson, N., Bommer, J. J., Scherbaum, F., Cotton, F., and Kuehn, N.: The variability of ground-motion prediction models and its components, Seismological Research Letters, 81, 794–801, 2010.

Basili, R., Brizuela, B., Herrero, A., Iqbal, S., Lorito, S., Maesano, F. E., Murphy, S., Perfetti, P., Romano, F., Scala, A., et al.: NEAMTHM18 documentation: the making of the TSUMAPS-NEAM tsunami hazard model 2018, 2019.

Basili, R., Brizuela, B., Herrero, A., Iqbal, S., Lorito, S., Maesano, F. E., Murphy, S., Perfetti, P., Romano, F., Scala, A., et al.: The making of the NEAM tsunami hazard model 2018 (NEAMTHM18), Frontiers in Earth Science, 8, 753, 2021.

Beckman, P.: Urgent Computing: Exploring Supercomputing's New Role, CTWatch Quarterly, 4, 3–4, 2008.

Beckman, P., Nadella, S., Trebon, N., and Beschastnikh, I.: SPRUCE: A system for supporting urgent high-performance computing, in: Grid-Based Problem Solving Environments: IFIP TC2/WG 2.5 Working Conference on Grid-Based Problem Solving Environments: Implications for Development and Deployment of Numerical Software July 17–21, 2006, Prescott, Arizona, USA, pp. 295–311, Springer, 2007.

Bernardi, F., Lomax, A., Michelini, A., Lauciani, V., Piatanesi, A., and Lorito, S.: Appraising the Early-est earthquake monitoring system for tsunami alerting at the Italian Candidate Tsunami Service Provider, Natural Hazards and Earth System Sciences, 15, 2019–2036, 2015.

Bindi, D., Pacor, F., Luzi, L., Puglia, R., Massa, M., Ameri, G., and Paolucci, R.: Ground motion prediction equations derived from the Italian strong motion database, Bulletin of Earthquake Engineering, 9, 1899–1920, 2011.

Boore, D. M., Stewart, J. P., Seyhan, E., and Atkinson, G. M.: NGA-West2 equations for predicting PGA, PGV, and 5% damped PSA for shallow crustal earthquakes, Earthquake Spectra, 30, 1057–1085, 2014.

Campbell, K. W. and Bozorgnia, Y.: NGA-West2 ground motion model for the average horizontal components of PGA, PGV, and 5% damped linear acceleration response spectra, Earthquake Spectra, 30, 1087–1115, 2014.

Cauzzi, C., Faccioli, E., Vanini, M., and Bianchini, A.: Updated predictive equations for broadband (0.01–10 s) horizontal response spectra and peak ground motions, based on a global dataset of digital acceleration records, Bulletin of Earthquake Engineering, 13, 1587–1612, 2015.

Chiou, B. S.-J. and Youngs, R. R.: Update of the Chiou and Youngs NGA model for the average horizontal component of peak ground motion and response spectra, Earthquake Spectra, 30, 1117–1153, 2014.

Cordrie, L., Selva, J., Bernardi, F., and Tonini, R.: Using available and incoming data for reducing and updating seismic source ensembles for probabilistic tsunami forecasting (PTF) in early-warning and urgent computing, Tech. rep., Copernicus Meetings, 2023.

de la Puente, J., Rodriguez, J. E., Monterrubio-Velasco, M., Rojas, O., and Folch, A.: Urgent supercomputing of earthquakes: Use case for civil protection, in: Proceedings of the platform for advanced scientific computing conference, pp. 1–8, 2020.

Douglas, J.: Earthquake ground motion estimation using strong-motion records: a review of equations for the estimation of peak ground acceleration and response spectral ordinates, Earth-Science Reviews, 61, 43–104, 2003.

Douglas, J.: Assessing the epistemic uncertainty of ground-motion predictions, in: Proceedings of the ninth US National and 10th Canadian conference on earthquake engineering, July, pp. 25–29, 2010a.

Douglas, J.: Consistency of ground-motion predictions from the past four decades, Bulletin of Earthquake Engineering, 8, 1515–1526, 2010b.

Douglas, J.: Ground motion prediction equations 1964–2020, Dept. Civil Environ. Eng., Univ Strathclyde, Glaskow, UK, p. 670, 2020.

Douglas, J. and Aochi, H.: A survey of techniques for predicting earthquake ground motions for engineering purposes, Surveys in geophysics, 29, 187–220, 2008.

Ejarque, J., Badia, R. M., Albertin, L., Aloisio, G., Baglione, E., Becerra, Y., Boschert, S., Berlin, J. R., D'Anca, A., Elia, D., et al.: Enabling dynamic and intelligent workflows for HPC, data analytics, and AI convergence, Future generation computer systems, 134, 414–429, 2022.

Engler, D. T., Worden, C. B., Thompson, E. M., and Jaiswal, K. S.: Partitioning ground motion uncertainty when conditioned on station data, Bulletin of the Seismological Society of America, 112, 1060–1079, 2022.

Feenstra, J. F.: Handbook on methods for climate change impact assessment and adaptation strategies, 1998.

Folch, A., Abril, C., Afanasiev, M., Amati, G., Bader, M., Badia, R. M., Bayraktar, H. B., Barsotti, S., Basili, R., Bernardi, F., et al.: The EU Center of Excellence for Exascale in Solid Earth (ChEESE): Implementation, results, and roadmap for the second phase, Future Generation Computer Systems, 146, 47–61, 2023.

Gasparini, P., Manfredi, G., Zschau, J., et al.: Earthquake early warning systems, Springer, 2007.

Gneiting, T. and Raftery, A. E.: Weather forecasting with ensemble methods, Science, 310, 248–249, 2005.

Grandinetti, L.: High performance computing and grids in action, vol. 16, IOS Press, 2008.

Guérin-Marthe, S., Gehl, P., Negulescu, C., Auclair, S., and Fayjaloun, R.: Rapid earthquake response: The state-of-the art and recommendations with a focus on European systems, International Journal of Disaster Risk Reduction, 52, 101 958, 2021.

Jia, Z., Jin, Z., Marchandon, M., Ulrich, T., Gabriel, A.-A., Fan, W., Shearer, P., Zou, X., Rekoske, J., Bulut, F., et al.: The complex dynamics of the 2023 Kahramanmaraş, Turkey, M w 7.8-7.7 earthquake doublet, Science, p. eadi0685, 2023.

Leonard, M.: Self-consistent earthquake fault-scaling relations: Update and extension to stable continental strike-slip faults, Bulletin of the Seismological Society of America, 104, 2953–2965, 2014.

Leong, S. H. and Kranzlmüller, D.: Towards a general definition of urgent computing, Procedia Computer Science, 51, 2337–2346, 2015.

Michelini, A., Faenza, L., Lanzano, G., Lauciani, V., Jozinović, D., Puglia, R., and Luzi, L.: The new ShakeMap in Italy: Progress and advances in the last 10 yr, Seismological Research Letters, 91, 317–333, 2020.

Molteni, F., Buizza, R., Palmer, T. N., and Petroliagis, T.: The ECMWF ensemble prediction system: Methodology and validation, Quarterly journal of the royal meteorological society, 122, 73–119, 1996.

Murphy, A. H.: What is a good forecast? An essay on the nature of goodness in weather forecasting, Weather and forecasting, 8, 281–293, 1993.

Pagani, M., Monelli, D., Weatherill, G., Danciu, L., Crowley, H., Silva, V., Henshaw, P., Butler, L., Nastasi, M., Panzeri, L., et al.: OpenQuake engine: An open hazard (and risk) software for the global earthquake model, Seismological Research Letters, 85, 692–702, 2014a.

Pagani, M., Monelli, D., Weatherill, G., and Garcia, J.: The OpenQuake-engine book: hazard, Global Earthquake Model (GEM) Technical Report, 8, 67, 2014b.

Selva, J., Tonini, R., Molinari, I., Tiberti, M. M., Romano, F., Grezio, A., Melini, D., Piatanesi, A., Basili, R., and Lorito, S.: Quantification of source uncertainties in seismic probabilistic tsunami hazard analysis (SPTHA), Geophysical Journal International, 205, 1780–1803, 2016.

Selva, J., Bernardi, F., Michelini, A., Romano, F., and Tonini, R.: D6. 2 Description of the use cases for Pillar III, 2021a.

Selva, J., Lorito, S., Volpe, M., Romano, F., Tonini, R., Perfetti, P., Bernardi, F., Taroni, M., Scala, A., Babeyko, A., et al.: Probabilistic tsunami forecasting for early warning, Nature communications, 12, 5677, 2021b.

Sparks, R. S. J.: Forecasting volcanic eruptions, Earth and Planetary Science Letters, 210, 1–15, 2003.

Taroni, M. and Selva, J.: A testable worldwide earthquake faulting mechanism model, Seismological Research Letters, 92, 3577–3585, 2021.

Team, C. W.: Good practice guidance paper on assessing and combining multi model climate projections, in: IPCC Expert meeting on assessing and combining multi model climate projections, p. 1, 2010.

Worden, C., Thompson, E., Hearne, M., and Wald, D.: ShakeMap Manual Online: technical manual, user's guide, and software guide, US Geological Survey, 2020.

Worden, C. B., Thompson, E. M., Baker, J. W., Bradley, B. A., Luco, N., and Wald, D. J.: Spatial and spectral interpolation of ground-motion intensity measure observations, Bulletin of the Seismological Society of America, 108, 866–875, 2018.

Zhao, J. X., Zhou, S., Zhou, J., Zhao, C., Zhang, H., Zhang, Y., Gao, P., Lan, X., Rhoades, D., Fukushima, Y., et al.: Ground-motion prediction equations for shallow crustal and upper-mantle earthquakes in Japan using site class and simple geometric attenuation functions, Bulletin of the Seismological Society of America, 106, 1552–1569, 2016.